ACS OMEGA

http://pubs.acs.org/journal/acsodf

Article

Optically Tunable Tin Oxide-Coated Hollow Gold−Silver Nanorattles for Use in Solar-Driven Applications

Chien-Hung Li,[#] Orawan Khantamat,[#] Tingting Liu, Md Masud Parvez Arnob, Li Lin, Andrew C. Jamison, Wei-Chuan Shih, Tai-Chou Lee, and T. Randall Lee*

Cite This: *ACS Omega* 2020, 5, 23769−23777

Read Online

ACCESS | Metrics & More | Article Recommendations | Supporting Information

ABSTRACT: Core@shell metal nanoparticles have emerged as promising photocatalysts because of their strong and tunable plasmonic properties; however, marked improvements in photocatalytic efficiency are needed if these materials are to be widely used in practical applications. Accordingly, the design of new and functional light-responsive nanostructures remains a central focus of nanomaterial research. To this end, we report the synthesis of nanorattles comprising hollow gold−silver nanoshells encapsulated within vacuous tin oxide shells of adjustable thicknesses (∼10 and ∼30 nm for the two examples prepared in this initial report). These composite nanorattles exhibited broad tunable optical extinctions ranging from ultraviolet to near-infrared spectral regions (i.e., 300−745 nm). Zeta potential measurements showed a large negative surface charge of approximately −35 mV, which afforded colloidal stability to the nanorattles in aqueous solution. We also characterized the nanorattles structurally and compositionally using scanning electron microscopy, transmission electron microscopy, and energy-dispersive X-ray spectroscopy. Futhermore, finite-difference time-domain simulation and photoluminescence properties of the composited nanoparticles were investigated. Collectively, these studies indicate that our tin oxide-coated hollow gold−silver nanorattles are promising candidates for use in solar-driven applications.

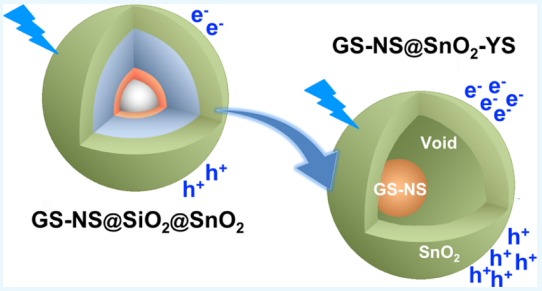

INTRODUCTION

Nanorattles or yolk−shell nanoparticles (yolk−shell NPs) are an interesting permutation of typical nanoshells that produce unique properties with their movable cores, interstitial hollow spaces, and alternative functionalities for the outer shells.[1] These unique properties provide nanorattles with significant potential as drug-delivery agents,[1] catalysts,[2−5] and energy-storage units in lithium-ion batteries.[6,7] Recent research efforts have included the development of metal nanoparticles as the core (the yolk) with semiconductor oxide materials as the shell, leading to nanorattles such as Au@TiO_2,[2] Au@SiO_2,[8] Au@Cu_2O,[9] Au@Fe_3O_4,[10] Au@CdS,[11] and Au@g-C_3N_4/SnS,[12] where selected examples exhibit promising photocatalytic activities.[2,11,12]

For research on these nanostructures, the unusual character of the core typically becomes the focus of attention, but the role of the shell as a means of controlling electron transmission has also gained interest. Tin oxide (SnO_2) is an attractive n-type semiconductor material with a wide band gap (∼3.6 eV) that exhibits a faster rate for the mobility of charge carriers than some of the other semiconductor materials such as TiO_2; moreover, SnO_2-based materials enjoy relatively slow rates of charge recombination,[13] which can offer enhanced photocatalytic activity in various systems. A recent study has shown that SnO_2-coated gold nanoparticles exhibit remarkable stability over a wide range of pH conditions.[14] This increased stability is needed for applications where the photoactive component must tolerate potentially harsh environments such as those found in solar energy applications and sensing devices.[15,16]

Another advantage associated with tin oxide is that as a semiconductor, its conduction band electrons readily interact with photons whose frequency is in resonance with the natural frequency of these surface electrons, enabling the absorption of this photon energy, a phenomenon known as surface plasmon resonance.[17] Notably, however, the localized surface plasmon resonance (LSPR) of SnO_2 nanoparticles responds to light at ultraviolet (UV) wavelengths.[18,19] Recent efforts have focused on increasing the range of wavelengths that SnO_2 can absorb by incorporating dopants in the SnO_2 matrix to adjust the electron density of the materials in order to shift the SPR band to the longer wavelength such as the near or mid-infrared (mid-IR) region.[19−22] A slightly different approach has been pursued by researchers who have encapsulated SPR-active

Received: June 13, 2020
Accepted: August 25, 2020
Published: September 11, 2020

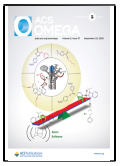

Scheme 1. Strategy for Synthesizing Tin Oxide-Coated Hollow Gold−Silver Nanorattles

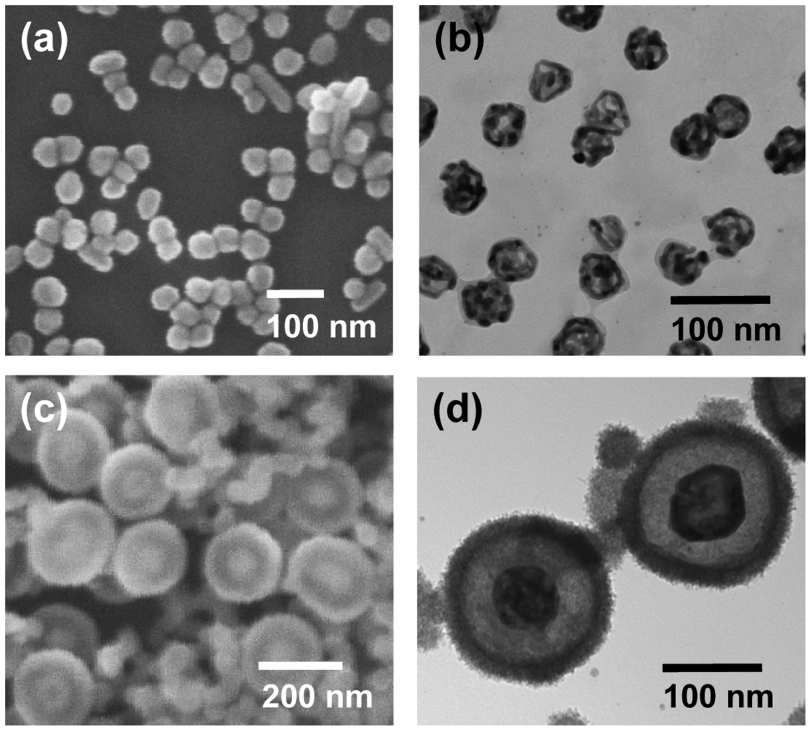

Figure 1. (a) SEM image of the Ag nanoparticles and (b) TEM image of hollow gold−silver nanoshells (GS-NS); (c) SEM and (d) TEM images of the GS-NS@SiO_2@SnO_2 nanoparticles formed when base was omitted during the final step in the synthesis of the nanorattles.

materials such as gold nanoparticles within a tin oxide shell to shift the absorption maxima for the gold surface.[23]

The groundwork for the pursuit of plasmonically enhanced solar-to-fuel cell energy collection working with unique nanostructures can be found in recent reports.[24,25] In most investigations, researchers have been utilizing materials that are SPR-active in the ultraviolet−visible light spectrum (~54% of sunlight) for photocatalytic reactions,[15,26−29] although there are some reports describing photocatalytic reactions activated by near-IR light (~46% of sunlight).[29−31] Relevant to our efforts in this area, Vongsavat et al. demonstrated a two-step synthesis procedure for the fabrication of hollow gold−silver nanoshells having an SPR band that extended across the visible and into the near-IR range.[32] More recent investigations involving these nanostructures explored porous silica-coated hollow gold−silver nanoshells that exhibited a broad range of optical properties from the visible to near-IR with remarkable stability when exposed to a wide range of pH conditions.[33] In separate studies, these nanoshells were used in conjunction with a $ZnInS_2$ photocatalyst in the water-splitting reaction, more than doubling the rate of hydrogen production when compared to the $ZnInS_2$ photocatalyst alone.[34] Interestingly, noncentrosymmetric Au−SnO_2 hybrid structures have demonstrated even greater photocatalytic enhancement because of the stronger localization of the plasmonic coupling between the interface of the metal and that of the semiconductor; moreover, this enhancement could be broadened by tuning the composition of the materials used.[35,36]

In the current investigation, we combine the advantages of hollow gold−silver nanoshells and tin oxide coatings in the design and study of noncentrosymmetric tin oxide-coated hollow gold−silver nanorattles. Scheme 1 illustrates the strategy used to prepare the tin oxide-coated hollow gold−silver nanorattles (GS-NS@SnO_2 nanorattles). First, we synthesized monodisperse silver nanoparticles (Ag NPs)[37] and then formed hollow gold−silver nanoshells by adding a custom-developed gold salt solution, displacing silver via galvanic replacement. Second, we coated the resultant hollow gold−silver nanoshells (GS-NS) with a thin shell of silica using sol−gel methods. In the last step, we added aqueous base to etch/remove the silica while concurrently adding a tin precursor to form a tin oxide shell via a modified hydrothermal method.[3] The resulting GS-NS@SnO_2 nanorattles exhibited a strong extinction band ranging from UV−visible to near-infrared wavelengths.

RESULTS AND DISCUSSION

Synthesis of the Nanorattles. The strategy used to prepare our tin oxide-coated hollow gold−silver nanorattles is illustrated above in Scheme 1. The first step required the synthesis of monodisperse silver nanoparticles, which was accomplished by using a modified citrate reduction method;[37] ascorbic acid was mixed with sodium citrate to increase the reduction rate, and the addition of I^- suppressed nanocrystal growth along the (111) facet. For the second step, we followed the method of Vongsavat et al. for preparing hollow gold−

https://dx.doi.org/10.1021/acsomega.0c02818
ACS Omega 2020, 5, 23769−23777

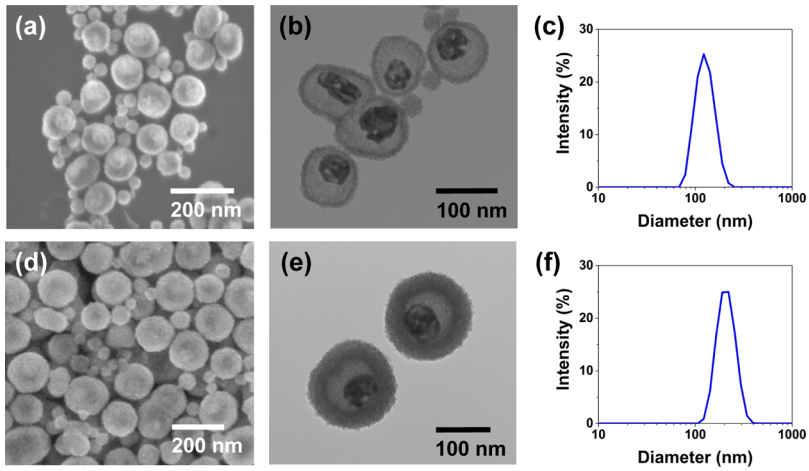

Figure 2. Morphology and size distribution of the GS-NS@SnO_2 nanorattles. (a) SEM, (b) TEM, and (c) DLS data of the GS-NS@SnO_2 nanorattles with a thin ~10 nm SnO_2 shell (GS-NS@SnO_2-YS(10)); (d) SEM, (e) TEM, and (f) DLS data of the GS-NS@SnO_2 nanorattles with a thick ~30 nm SnO_2 shell (GS-NS@SnO_2-YS(30)).

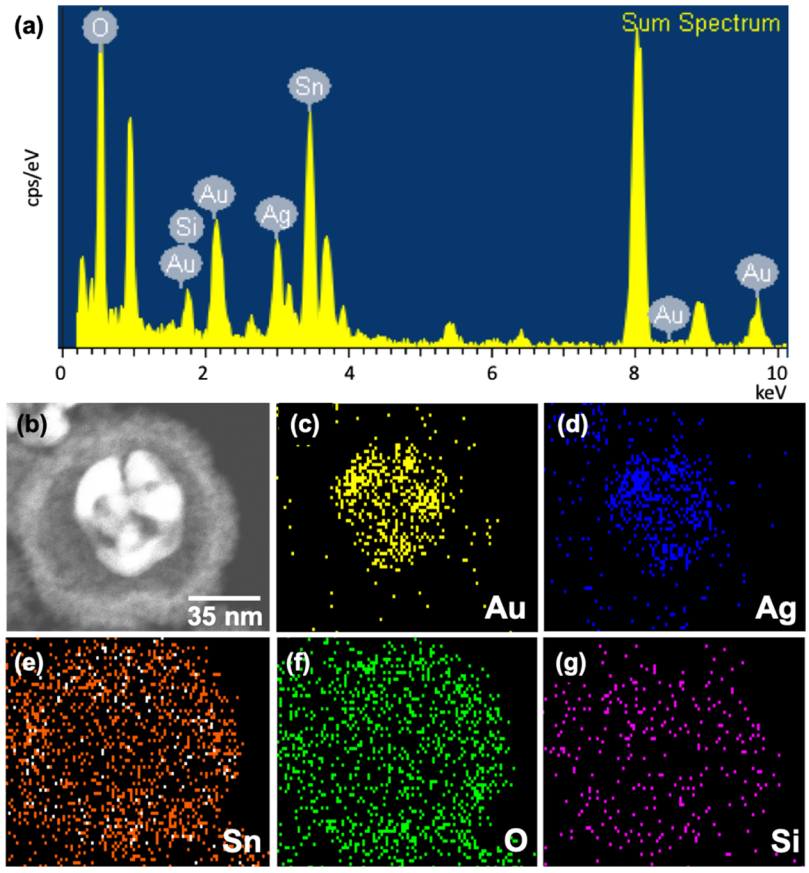

Figure 3. Compositional analysis of the GS-NS@SnO_2-YS(10) nanorattles: (a) EDX profile and (b) STEM image of an individual GS-NS@SnO_2-YS(10) nanorattle, and the EDX mapping images of (c) Au, (d) Ag, (e) Sn, (f) O, and (g) Si.

silver nanoshells (GS-NS) via galvanic replacement by adding gold salt solution to the silver nanoparticles. Figure 1a provides a scanning electron microscopy (SEM) image of the uniform silver nanoparticles, and Figure 1b shows a transmission electron microscopy (TEM) image of the uniform hollow gold−silver nanoshells used subsequently to produce the nanorattles. The size of these nanoshell cores is ~55 nm in diameter. With the third step, we used a standard sol−gel method to coat the hollow gold−silver nanoshells with a thin silica layer under slightly basic conditions. In the next step, we used the silica shell as a template for coating the composite nanoparticles with tin oxide; notably, without adding base in this step, the silica layer remains to form a triple layered structure (GS-NS@SiO_2@SnO_2), where tin oxide is the outer layer, silica is an interlayer, and the gold−silver nanoshells provide the core structure (see Figure 1c,d). For this step, prior reports indicate that hydrolysis of the urea generates carbon dioxide, as shown in eq 1,[3] and carbon dioxide then

https://dx.doi.org/10.1021/acsomega.0c02818
ACS Omega 2020, 5, 23769−23777

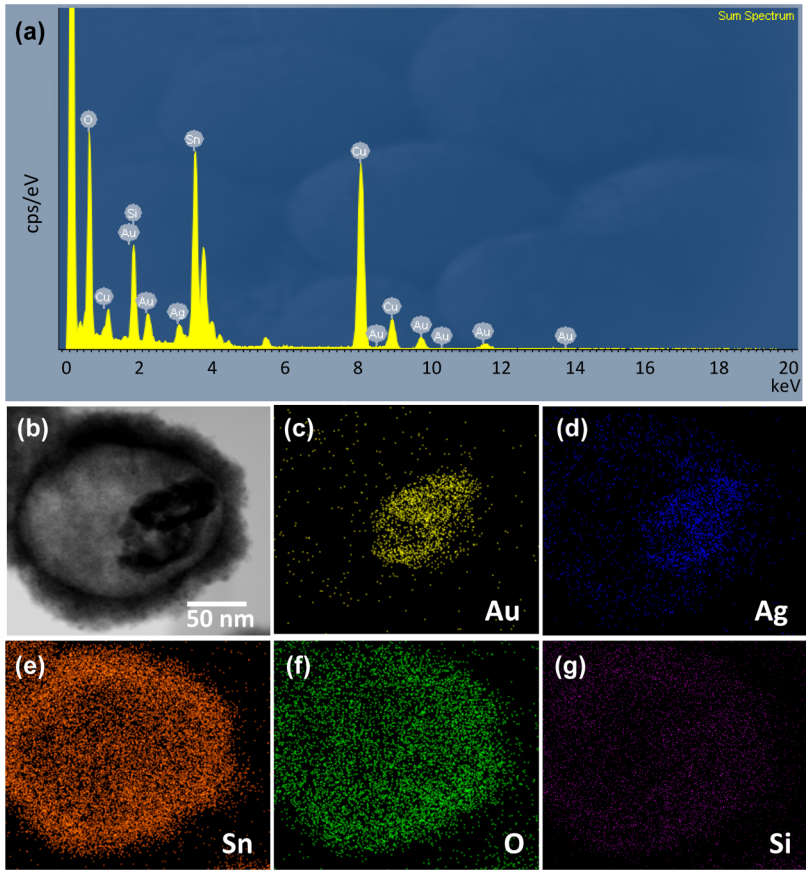

Figure 4. Compositional analysis of the GS-NS@SnO_2-YS(30) nanorattles: (a) EDX profile and (b) TEM image of an individual GS-NS@SnO_2-YS(30) nanorattle, and the EDX mapping images of (c) Au, (d) Ag, (e) Sn, (f) O, and (g) Si.

reacts with the tin precursor compound to produce the tin oxide shell, as shown in eq 2. We also note that the addition of base in this step leads to an increase in pH, which enhances the solubility of SiO_2 and consequently generates void space between the GS-NS core and the SnO_2 shell.[38]

$$CO(NH_2)_2 + H_2O \rightarrow CO_2 + NH_3 \quad (1)$$

$$Na_2SnO_3{\cdot}3H_2O + CO_2 \rightarrow SnO_2 + 3H_2O + Na_2CO_3 \quad (2)$$

Size, Morphology, and Surface Charge of the Nanorattles. Importantly, when the tin oxide coating procedure is conducted under basic conditions, the silica layer is etched and largely removed to afford the nanorattle structure. Figure 2a,b shows the SEM and TEM images of the GS-NS@SnO_2 nanorattles coated with a thin tin oxide shell (~10 nm), yielding a composite nanoparticle of ~110 nm in diameter. Similarly, Figure 2d,e shows the SEM and TEM images of the GS-NS@SnO_2 nanorattles coated with a thicker tin oxide shell (~30 nm), producing a composite nanoparticle of ~140 nm in diameter. All of the images of the nanorattles demonstrate that the tin oxide shell remains intact after etching of the silica interlayer and contains independent hollow gold–silver nanoshells in the void space within the tin oxide shell.

Figure 2c,f shows the size distribution data collected using dynamic light scattering (DLS) for the GS-NS@SnO_2-YS(10) and GS-NS@SnO_2-YS(30) samples. The average particle diameters of 123 nm for GS-NS@SnO_2-YS(10) and 203 nm for GS-NS@SnO_2-YS(30) are higher than the values determined from the SEM and TEM images, as shown in Figure 2, which can be attributed to the fact that DLS measures the hydrodynamic diameter rather than the actual physical diameter of the nanoparticles. In addition, we obtained zeta potential measurements to determine the surface charge/electric potential on our nanorattles in aqueous solution. The average surface charges for the nanorattles were measured to be −36 and −35 mV for GS-NS@SnO_2-YS(10) and GS-NS@SnO_2-YS(30), respectively, which indicates that there is a negative charge distribution on the surface of the tin oxide shells. The high negative charge can prevent aggregation[39] and is consistent with our observation that the nanorattles are colloidally stable in aqueous solution.

EDX Elemental Analysis and TEM Mapping of the Nanorattles. The energy-dispersive spectrometry (EDX) spectra and elemental mapping of the GS-NS@SnO_2-YS(10) and GS-NS@SnO_2-YS(30) nanorattles confirmed the presence Ag and Au for the core structure, Sn for the tin oxide shell, O as part of the oxide, and residual Si, as shown in Figure 3 and 4. The peak for Cu in the spectra at ~8 keV can be attributed to the TEM grids. Notably, the small but evident peak for Si probably arises from residual silica that was resistant to etching under the mild conditions employed. Quantitatively, Table S1 in the Supporting Information provides the Si/Sn ratio for the samples of GS-NS@SiO_2@SnO_2 (10 nm SnO_2 shell), GS-NS@SnO_2-YS(10), and GS-NS@SnO_2-YS(30). Importantly, the Si/Sn ratio changes from 2.0 to 0.2 to 0.5, as the silica is etched out, and the thickness of the tin oxide shell is increased. The EDX spectrum and elemental mapping of the GS-NS@SiO_2@SnO_2 nanoparticles are provided in Figure S1 in the Supporting Information. Comparison of the EDX data as a

https://dx.doi.org/10.1021/acsomega.0c02818
ACS Omega 2020, 5, 23769−23777

whole confirms that the composition of the nanoparticles is consistent with the chemical procedures to which they were subjected.

Extinction Spectra of the Nanorattles. Figure 5 shows the extinction spectra for the silica-coated hollow gold−silver

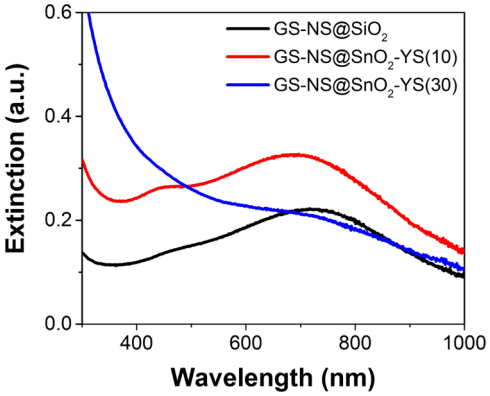

Figure 5. UV−vis spectra for the silica-coated hollow gold−silver nanoshells and the two types of tin oxide-coated hollow gold−silver nanorattles.

nanoshells (GS-NS@SiO_2) and the two different types of tin oxide-coated hollow gold−silver nanorattles: thin-shelled GS-NS@SnO_2-YS(10) and thick-shelled GS-NS@SnO_2-YS(30). Notably, the spectral features for the silica-coated hollow gold−silver nanoshells (black line) and those for the thin-shelled tin oxide-coated nanorattles (red line) are similar: the extinction peaks extend from the visible (∼400 nm) to the near-infrared (∼1000 nm), and the maximum intensity appears at ∼745 nm; in addition, the small peak at ∼450 nm likely arises from the quadruple mode of the LSPR of the nanoshells.[40] When comparing these two nanomaterials, the peak intensity of the nanorattles in the visible region shows a slight blue shift as compared to the silica-coated nanoshells, a shift that might be because of small molecules such as water or ethanol penetrating into the tin oxide shell and filling the void space surrounding the gold−silver nanoshells.[8] For the materials involved, the refractive index of water is 1.33,[41] which is smaller than silica at 1.46 and tin oxide at 2.2.[42,43]

In contrast to the nanoshells (black line) and the thin-shelled tin oxide-coated nanorattles (red line), the thick-shelled tin oxide-coated nanorattles (blue line) exhibited a broad strong extinction in the UV range, with muted contributions from the nanoshell core tailing into the visible and near-infrared, which can be attributed to scattering by the thicker tin oxide shell.[8] On the whole, the nanorattles demonstrate a broad optical absorption/scattering band that offers potential for enhanced light absorption for photocatalytic systems, particularly when the tin oxide shell is thin.

Photoluminescence Emission Spectra of the Nanorattles. We utilized photoluminescence (PL) emission spectroscopy to investigate the efficiency of charge transfer for our composite nanoparticles. We used an excitation wavelength of 300 nm for the excitation of the SnO_2 nanoparticles in this study. Figure 6 shows the PL intensities of the GS-NS@SiO_2@SnO_2 nanoshells and the GS-NS@SnO_2-YS nanorattles, where lower PL intensity corresponds to lower recombination probability for the SnO_2 nanoparticles. Interestingly, the GS-NS@SnO_2-YS(10) nanorattles showed the lowest intensity emission peak at ∼375 nm, indicating the

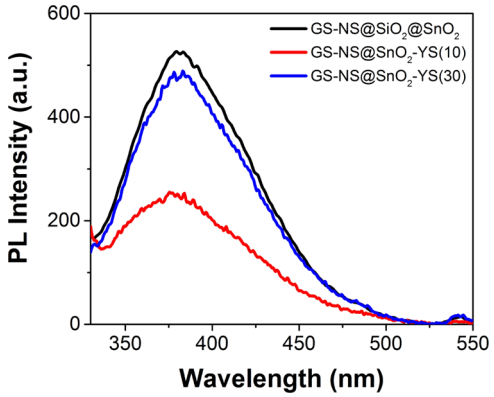

Figure 6. Photoluminescence (PL) emission spectra of GS-NS@SiO_2@SnO_2 nanoshells (black), GS-NS@SnO_2-YS(10) nanorattles (red), and GS-NS@SnO_2-YS(30) nanorattles (blue).

possibility of electrons transferring from SnO_2 to the GS-NS, which can be interpreted as a diminished/inhibited recombination process in these nanorattles. However, we observed no significant differences between the GS-NS@SnO_2-YS(30) nanorattles and the GS-NS@SiO_2@SnO_2 nanoshells, as both of these latter composite nanoparticles possessed thick dielectric shells surrounding the GS-NS core and exhibited high charge and hole recombination rates. Based on these results, the GS-NS@SnO_2-YS(10) nanorattles appear to be the best candidates for use in photocatalytic reactions.

Simulation of Electromagnetic Field of the GS-NS@SnO_2 Nanorattles. To gain a deeper understanding of the electromagnetic field distribution of the nanorattles, we performed finite-difference time-domain (FDTD) simulations for both horizontal and vertical polarizations of the three types of composite nanoparticles studied (see Figure 7). FDTD simulations (also known as Yee's method for solving Maxwell's equations)[44] are often used to understand the near-field enhancements observed for composite plasmonic nanoparticles such as gold−silver alloy nanoparticles, Ag@SiO_2 nanoparticles, and Au@SiO_2 nanoparticles.[45,46] Regarding to the horizontal electromagnetic field distribution, we observed stronger electromagnetic field enhancement at the side of the tin oxide shell in contact with the GS-NS (Figure 7c,e) in comparison to the GS-NS@SiO_2@SnO_2 core−shell structure (Figure 7a); this result is consistent with that found in prior studies of noncentrosymmetric metal−semiconductor hybrid structures.[34] Importantly, the GS-NS@SnO_2-YS(10) nanorattles showed stronger electromagnetic field enhancement than the GS-NS@SnO_2-YS(30) nanorattles. However, we observed no significant differences in the vertical electromagnetic field distribution for this series of composite nanoparticles (see Figure 7b,d,f). Overall, the simulation results are consistent with the PL results above in indicating that the GS-NS@SnO_2-YS(10) nanorattles are the most promising candidates for use in photocatalytic reactions.

CONCLUSIONS

Tin oxide-coated hollow gold−silver nanorattles with uniform sizes and spherical shapes were synthesized and characterized by SEM, TEM, DLS, zeta potential, UV−vis, EDX, PL, and electromagnetic field simulations. The collective results indicate that these nanorattle structures, which contain hollow gold−silver nanoshells within the void space of their stable tin oxide shells, are attractive new materials for use in solar-driven

https://dx.doi.org/10.1021/acsomega.0c02818
ACS Omega 2020, 5, 23769−23777

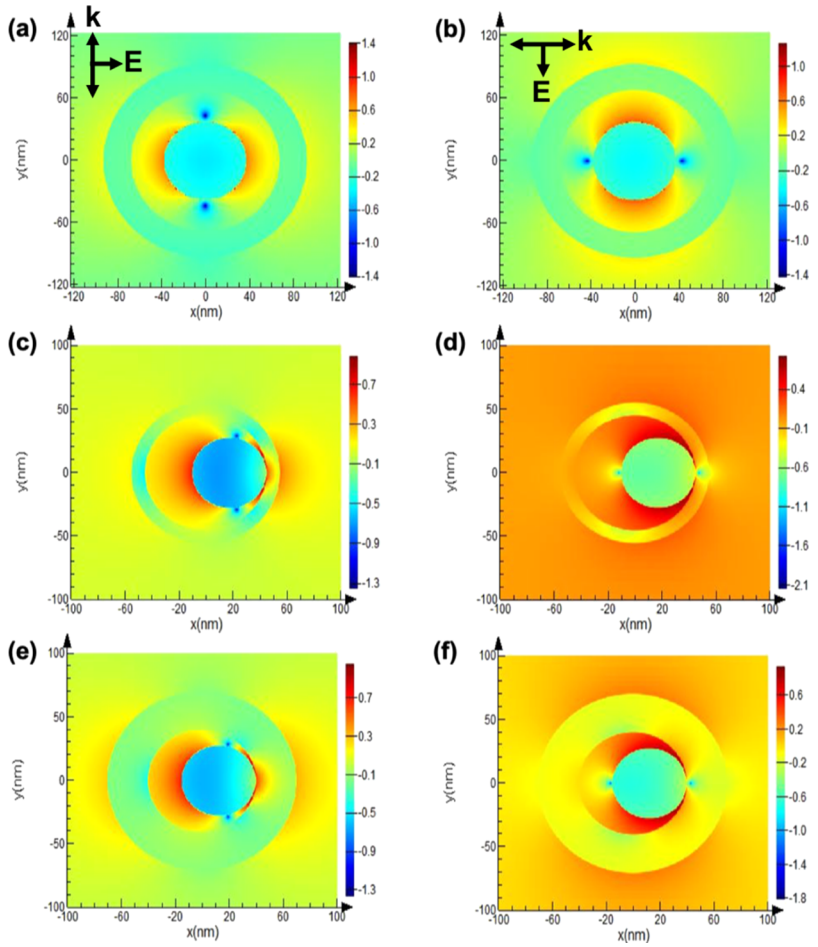

Figure 7. Calculated electric field enhancement at 750 nm for (a,b) GS-NS@SiO_2@SnO_2, (c,d) GS-NS@SnO_2-YS(10), and (e,f) GS-NS@SnO_2-YS(30).

applications, with strong optical extinctions ranging from visible to near-infrared wavelengths. Investigations involving the use of these nanorattles in solar-to-fuel photocatalytic conversion are currently underway in our laboratory.

EXPERIMENTAL SECTION

Materials. Silver nitrate ($AgNO_3$; Aldrich), trisodium citrate dihydrate (NaCit; EM Science), potassium iodide (KI; J. T. Baker), L-ascorbic acid ($C_6H_8O_6$; Aldrich), potassium carbonate (K_2CO_3; Aldrich), hydrogen tetrachloroaurate(III) hydrate ($HAuCl_4·H_2O$; Strem), Urea (NH_2CONH_2; Mallinckrodt Chemicals), sodium stannate trihydrate ($Na_2SnO_3·3H_2O$; Aldrich), nitric acid (HNO_3; EM Science), hydrochloric acid (HCl; EM Science), ammonium hydroxide (NH_4OH; EM science), sodium hydroxide (NaOH; EM Science), and tetraethylorthosilicate (TEOS, Aldrich) were purchased from the indicated suppliers and used without modification. Water was purified to a resistance of 18 MΩ (Academic Milli-Q Water System; Millipore Corporation) and filtered using a 0.22 μm filter. All glasswares used in the experiments were cleaned in an aqua regia solution (3:1 HCl/HNO_3) and dried in the oven prior to use.

Preparation of Silver Nanoparticle Cores. Silver nanoparticles were prepared using a modified citrate reduction method reported by Li et al.[37] The first step in this procedure was to combine 600 μL of 2.5 mM ascorbic acid with 95 mL of water in a 250 mL round bottom flask, which was then stirred and heated to boiling. At the same time, 0.0167 g of $AgNO_3$ (0.0100 mmol) was added to 3 mL of water, 2 mL of 1% sodium citrate, and 100 μL of 1% KI in a small centrifuge tube and allowed to sit for 15 min. After 15 min, the contents of the centrifuge tube were added to the round bottom flask, and the mixture was refluxed for 1 h. A brownish yellow color was observed, which is consistent with the presence of silver nanoparticles. The solution was allowed to cool to rt and was then centrifuged at 7000 rpm for 15 min. After removing the supernatant, the residue was redispersed in 12.5 mL of purified water.

Preparation of Hollow Gold−Silver Nanoshells. To produce the hollow gold−silver nanoshells (GS-NS), a basic solution of gold salt (K-gold solution) was prepared using the method reported by Oldenburg et al.[47] Specifically, 0.025 g of potassium carbonate (K_2CO_3) was added to 100 mL of Milli-Q water, which was then infused with 2 mL of 1% $HAuCl_4·H_2O$ solution. The mixture, which was initially yellow, became colorless 30 min after the reaction was initiated. The flask was then covered with aluminum foil to shield it from light, and the solution was stored in a refrigerator overnight. An aliquot (10 mL) of silver nanoparticle solution prepared as described above was mixed with 100 mL of K-gold solution and stirred for another 5 h until the SPR band reached ∼800 nm. The resulting particle solution was then centrifuged at 7000 rpm for

https://dx.doi.org/10.1021/acsomega.0c02818
ACS Omega 2020, 5, 23769−23777

15 min, and the supernatant was decanted. The residue was redispersed in 20 mL of purified water.

Preparation of Silica-Coated Hollow Gold−Silver Nanoshells. The silica-coating process for the gold−silver nanoshells (GS-NS@SiO_2) was adapted from the Stöber method.[48] The 20 mL portion of gold−silver nanoshell solution prepared in the prior step was mixed with ammonium hydroxide (2 mL) and ethanol (45 mL). Under vigorous stirring, 100 μL of TEOS was added to this solution. The mixture was then further stirred overnight at rt to allow the gold−silver nanoshells to be encapsulated within a thin silica layer. The solution was then centrifuged at 6000 rpm for 20 min. After removing the supernatant, the nanoshells were redispersed in 10 mL of purified water.

Preparation of Tin Oxide-Coated Hollow Gold−Silver Nanorattles. The tin oxide-coated hollow gold−silver nanorattle (GS-NS@SnO_2 nanorattles) synthesis procedure was optimized and adapted based on the hydrothermal method reported by Zhang et al.[3] The first step in this process was to mix 3 mL of the silica-coated hollow gold−silver nanoshell solution prepared above with 3 mL of absolute ethanol in a 50-mL glass pressure vessel. Concurrently, 0.2 mL of 0.2 M urea, 0.4 mL of 0.08 M sodium stannate trihydrate, and 50 μL of 0.1 M NaOH were added. As reported previously,[14] silica-coated gold nanoparticles are unstable under basic conditions; correspondingly, to etch out the silica during the tin oxide-coating process,[38] we added the NaOH to adjust pH to ∼11. After stirring for 1 h, the temperature was increased to 135 °C, and the solution was stirred for another hour. The solution was then allowed to cool and was centrifuged at 6000 rpm for 15 min. After removing the supernatant, the residue was redispersed in ethanol. In addition, by varying the sodium stannate trihydrate concentration, the thickness of the tin oxide coating on the hollow gold−silver nanorattles could be varied.

FDTD Simulation Studies. Each FDTD simulation was performed for a single nanoparticle. The simulation domain was fixed at 2 μm × 2 μm × 2 μm. Perfectly matched layers were used on all the boundaries, with antisymmetric and symmetric boundary conditions for x min and y min. The effect of staircase approximation was addressed by reducing the mesh size around the nanoparticle to 0.5 nm × 0.5 nm × 0.5 nm. The surrounding refractive index was considered to be 1.36 (ethanol). The simulations were performed on a computer with 8-core calculation nodes, each carrying 4 GB of memory.

Characterization. The morphology of the obtained particles was evaluated using LEO-1525 SEM operating at an accelerating voltage of 15 kV. To obtain high-resolution SEM images, all samples were deposited on silicon wafers. Similarly, the size and morphology of the particles were evaluated by using JEM-2000 FX TEM operating at an accelerating voltage of 200 kV. All TEM samples were deposited on 300 mesh holey carbon-coated copper grids and dried overnight before analysis. UV−vis spectra were obtained using a Cary 50 Scan UV−visible spectrometer over the wavelength range of 200−1000 nm. DLS and zeta potential measurements were obtained using a Malvern Zetasizer Nano ZS90 instrument with dilute solutions of nanoparticles. EDX spectra were collected using JEOL JSM 6330F field-emission SEM equipped with an EDAX EDX detector using a TEAM computer-controlled system. Photoluminescence (PL) spectra were obtained using a PL spectrometer (PerkinElmer LS-55) with 300 nm incident light from a Xe flash lamp used for the excitation.

■ ASSOCIATED CONTENT

Supporting Information

The Supporting Information is available free of charge at https://pubs.acs.org/doi/10.1021/acsomega.0c02818.

Details on the atomic compositions of the composite nanoparticles determined by EDX and elemental mapping of the GS-NS@SiO_2@SnO_2 nanoshells (PDF)

■ AUTHOR INFORMATION

Corresponding Author

T. Randall Lee − *Department of Chemistry and the Texas Center for Superconductivity, University of Houston, Houston, Texas 77204, United States;* orcid.org/0000-0001-9584-8861; Email: trlee@uh.edu

Authors

Chien-Hung Li − *Department of Medicinal and Applied Chemistry, Kaohsiung Medical University, Kaohsiung 80708, Taiwan;* orcid.org/0000-0003-1643-8368

Orawan Khantamat − *Department of Biochemistry, Faculty of Medicine, Chiang Mai University, Chiang Mai 50200, Thailand*

Tingting Liu − *Department of Chemistry and the Texas Center for Superconductivity, University of Houston, Houston, Texas 77204, United States*

Md Masud Parvez Arnob − *Department of Electrical and Computer Engineering, University of Houston, Houston, Texas 77204, United States*

Li Lin − *Department of Medicinal and Applied Chemistry, Kaohsiung Medical University, Kaohsiung 80708, Taiwan*

Andrew C. Jamison − *Department of Chemistry and the Texas Center for Superconductivity, University of Houston, Houston, Texas 77204, United States*

Wei-Chuan Shih − *Department of Electrical and Computer Engineering, University of Houston, Houston, Texas 77204, United States*

Tai-Chou Lee − *Department of Chemical and Materials Engineering, National Central University, Jhongli City 32001, Taiwan;* orcid.org/0000-0002-1695-1201

Complete contact information is available at: https://pubs.acs.org/10.1021/acsomega.0c02818

Author Contributions

#C.-H.L. and O.K. contributed equally to this work.

Notes

The authors declare no competing financial interest.

■ ACKNOWLEDGMENTS

The authors thank the US Air Force (AFOSR FA2386-17-1-4028 and FA9550-18-1-0094), the Robert A. Welch Foundation (E-1320), and the Texas Center for Superconductivity for generously supporting this research. Additionally, the Malvern Nanosight instrument used in this study was acquired using a Defense University Research Instrumentation Program (DURIP) grant (FA9550-15-1-0374) issued by the Air Force Office of Scientific Research.

■ REFERENCES

(1) Liu, J.; Qiao, S. Z.; Hartono, S. B.; Lu, G. Q. M. Monodisperse Yolk-Shell Nanoparticles with a Hierarchical Porous Structure for

Delivery Vehicles and Nanoreactors. *Angew. Chem. Int. Ed.* **2010**, *49*, 4981−4985.
(2) Lee, I.; Joo, J. B.; Yin, Y.; Zaera, F. A Yolk@Shell Nanoarchitecture for Au/TiO_2 Catalysts. *Angew. Chem. Int. Ed.* **2011**, *50*, 10208−10211.
(3) Zhang, X.; Ren, H.; Wang, T.; Zhang, L.; Li, L.; Wang, C.; Su, Z. Controlled Synthesis and Magnetically Separable Photocatalytic Properties of Magnetic Iron Oxides@SnO_2 Yolk-Shell Nanocapsules. *J. Mater. Chem.* **2012**, *22*, 13380−13385.
(4) Yue, Q.; Li, J.; Zhang, Y.; Cheng, X.; Chen, X.; Pan, P.; Su, J.; Elzatahry, A. A.; Alghamdi, A.; Deng, Y.; Zhao, D. Plasmolysis-Inspired Nanoengineering of Functional Yolk−Shell Microspheres with Magnetic Core and Mesoporous Silica Shell. *J. Am. Chem. Soc.* **2017**, *139*, 15486−15493.
(5) Li, A.; Zhu, W.; Li, C.; Wang, T.; Gong, J. Rational Design of Yolk-Shell Nanostructures for Photocatalysis. *Chem. Soc. Rev.* **2019**, *48*, 1874−1907.
(6) Hong, Y. J.; Son, M. Y.; Kang, Y. C. One-Pot Facile Synthesis of Double-Shelled SnO_2 Yolk-Shell-Structured Powders by Continuous Process as Anode Materials for Li-ion Batteries. *Adv. Mater.* **2013**, *25*, 2279−2283.
(7) Liu, J.; Yu, L.; Wu, C.; Wen, Y.; Yin, K.; Chiang, F.-K.; Hu, R.; Liu, J.; Sun, L.; Gu, L.; Maier, J.; Yu, Y.; Zhu, M. New Nanoconfined Galvanic Replacement Synthesis of Hollow Sb@C Yolk−Shell Spheres Constituting a Stable Anode for High-Rate Li/Na-Ion Batteries. *Nano Lett.* **2017**, *17*, 2034−2042.
(8) Zhang, T.; Ge, J.; Hu, Y.; Zhang, Q.; Aloni, S.; Yin, Y. Formation of Hollow Silica Colloids through a Spontaneous Dissolution-Regrowth Process. *Angew. Chem. Int. Ed.* **2008**, *47*, 5806−5811.
(9) Zhang, L.; Blom, D. A.; Wang, H. Au-Cu_2O Core-Shell Nanoparticles: A Hybrid Metal-Semiconductor Heteronanostructure with Geometrically Tunable Optical Properties. *Chem. Mater.* **2011**, *23*, 4587−4598.
(10) Shevchenko, E. V.; Bodnarchuk, M. I.; Kovalenko, M. V.; Talapin, D. V.; Smith, R. K.; Aloni, S.; Heiss, W.; Alivisatos, A. P. Gold/Iron Oxide Core/Hollow-Shell Nanoparticles. *Adv. Mater.* **2008**, *20*, 4323−4329.
(11) Chiu, Y.-H.; Naghadeh, S. B.; Lindley, S. A.; Lai, T.-H.; Kuo, M.-Y.; Chang, K.-D.; Zhang, J. Z.; Hsu, Y.-J. Yolk-Shell Nanostructure as an Emerging Photocatalyst Paradigm for Solar Hydrogen Generation. *Nano Energy* **2019**, *62*, 289−298.
(12) Liang, M.; Borjigin, T.; Zhang, Y.; Liu, H.; Liu, B.; Guo, H. Z-Scheme Au@Void@g-C_3N_4/SnS Yolk-Shell Heterostructures for Superior Photocatalytic CO_2 Reduction under Visible Light. *ACS Appl. Mater. Interfaces* **2018**, *10*, 34123−34131.
(13) Dong, Z.; Ren, H.; Hessel, C. M.; Wang, J.; Yu, R.; Jin, Q.; Yang, M.; Hu, Z.; Chen, Y.; Tang, Z.; Zhao, H.; Wang, D. Quintuple-Shelled SnO_2 Hollow Microspheres with Superior Light Scattering for High-Performance DyeSensitized Solar Cells. *Adv. Mater.* **2014**, *26*, 905−909.
(14) Lee, S. H.; Rusakova, I.; Hoffman, D. M.; Jacobson, A. J.; Lee, T. R. Monodisperse SnO_2-Coated Gold Nanoparticles Are Markedly More Stable than Analogous SiO_2-Coated Gold Nanoparticles. *ACS Appl. Mater. Interfaces* **2013**, *5*, 2479−2484.
(15) Brown, M. D.; Suteewong, T.; Kumar, R. S. S.; D'Innocenzo, V.; Petrozza, A.; Lee, M. M.; Wiesner, U.; Snaith, H. J. Plasmonic Dye-Sensitized Solar Cells Using Core-Shell Metal-Insulator Nanoparticles. *Nano Lett.* **2011**, *11*, 438−445.
(16) Yu, Y.-T.; Dutta, P. Examination of Au/SnO_2 Core-Shell Architecture Nanoparticle for Low Temperature Gas Sensing Applications. *Sens. Actuators, B* **2011**, *157*, 444−449.
(17) Faucheaux, J. A.; Stanton, A. L. D.; Jain, P. K. Plasmon Resonances of Semiconductor Nanocrystals: Physical Principles and New Opportunities. *J. Phys. Chem. Lett.* **2014**, *5*, 976−985.
(18) Chandra, D.; Mukherjee, N.; Mondal, A.; Bhaumik, A. Design and Synthesis of Nanostructured Porous SnO_2 With High Surface Areas and their Optical and Dielectric Properties. *J. Phys. Chem. C* **2008**, *112*, 8668−8674.
(19) Xu, J. M.; Li, L.; Wang, S.; Ding, H. L.; Zhang, Y. X.; Li, G. H. Influence of Sb Doping on the Structural and Optical Properties of Tin Oxide Nanocrystals. *CrystEngComm* **2013**, *15*, 3296−3300.
(20) Kanehara, M.; Koike, H.; Yoshinaga, T.; Teranishi, T. Indium Tin Oxide Nanoparticles with Compositionally Tunable Surface Plasmon Resonance Frequencies in the Near-IR Region. *J. Am. Chem. Soc.* **2009**, *131*, 17736−17737.
(21) Lounis, S. D.; Runnerstrom, E. L.; Bergerud, A.; Nordlund, D.; Milliron, D. J. Influence of Dopant Distribution on the Plasmonic Properties of Indium Tin Oxide Nanocrystals. *J. Am. Chem. Soc.* **2014**, *136*, 7110−7116.
(22) Medhi, R.; Li, C.-H.; Lee, S. H.; Marquez, M. D.; Jacobson, A. J.; Lee, T.-C.; Lee, T. R. Uniformly Spherical and Monodisperse Antimony- and Zinc-Doped Tin Oxide Nanoparticles for Optical and Electronic Applications. *ACS Appl. Nano Mater.* **2019**, *2*, 6554−6564.
(23) Oldfield, G.; Ung, T.; Mulvaney, P. Au@SnO_2 Core-Shell Nanocapacitors. *Adv. Mater.* **2000**, *12*, 1519−1522.
(24) Linic, S.; Christopher, P.; Ingram, D. B. Plasmonic-Metal Nanostructures for Efficient Conversion of Solar to Chemical Energy. *Nat. Mater.* **2011**, *10*, 911−921.
(25) Thomann, I.; Pinaud, B. A.; Chen, Z.; Clemens, B. M.; Jaramillo, T. F.; Brongersma, M. L. Plasmon Enhanced Solar-to-Fuel Energy Conversion. *Nano Lett.* **2011**, *11*, 3440−3446.
(26) Cushing, S. K.; Li, J.; Meng, F.; Senty, T. R.; Suri, S.; Zhi, M.; Li, M.; Bristow, A. D.; Wu, N. Photocatalytic Activity Enhanced by Plasmonic Resonant Energy Transfer from Metal to Semiconductor. *J. Am. Chem. Soc.* **2012**, *134*, 15033−15041.
(27) Hou, W.; Hung, W. H.; Pavaskar, P.; Goeppert, A.; Aykol, M.; Cronin, S. B. Photocatalytic Conversion of CO_2 to Hydrocarbon Fuels via Plasmon-Enhanced Absorption and Metallic Interband Transitions. *ACS Catal.* **2011**, *1*, 929−936.
(28) Torimoto, T.; Horibe, H.; Kameyama, T.; Okazaki, K.-i.; Ikeda, S.; Matsumura, M.; Ishikawa, A.; Ishihara, H. Plasmon-Enhanced Photocatalytic Activity of Cadmium Sulfide Nanoparticle Immobilized on Silica-Coated Gold Particles. *J. Phys. Chem. Lett.* **2011**, *2*, 2057−2062.
(29) Ueno, K.; Misawa, H. Plasmon-Enhanced Photocurrent Generation and Water Oxidation from Visible to Near-Infrared Wavelengths. *NPG Asia Mater.* **2013**, *5*, No. e61.
(30) Nishijima, Y.; Ueno, K.; Kotake, Y.; Murakoshi, K.; Inoue, H.; Misawa, H. Near-Infrared Plasmon-Assisted Water Oxidation. *J. Phys. Chem. Lett.* **2012**, *3*, 1248−1252.
(31) Wang, F.; Li, C.; Chen, H.; Jiang, R.; Sun, L.-D.; Li, Q.; Wang, J.; Yu, J. C.; Yan, C.-H. Plasmonic Harvesting of Light Energy for Suzuki Coupling Reactions. *J. Am. Chem. Soc.* **2013**, *135*, 5588−5601.
(32) Vongsavat, V.; Vittur, B. M.; Bryan, W. W.; Kim, J.-H.; Lee, T. R. Ultrasmall Hollow Gold-Silver Nanoshells with Extinctions Strongly Red-Shifted to the Near-Infrared. *ACS Appl. Mater. Interfaces* **2011**, *3*, 3616−3624.
(33) Li, C.-H.; Jamison, A. C.; Rittikulsittichai, S.; Lee, T.-C.; Lee, T. R. In Situ Growth of Hollow Gold-Silver Nanoshells within Porous Silica Offers Tunable Plasmonic Extinctions and Enhanced Colloidal Stability. *ACS Appl. Mater. Interfaces* **2014**, *6*, 19943−19950.
(34) Li, C.-H.; Li, M.-C.; Liu, S.-P.; Jamison, A. C.; Lee, D.; Lee, T. R.; Lee, T.-C. Plasmonically Enhanced Photocatalytic Hydrogen Production from Water: The Critical Role of Tunable Surface Plasmon Resonance from Gold−Silver Nanoshells. *ACS Appl. Mater. Interfaces* **2016**, *8*, 9152−9161.
(35) Seh, Z. W.; Liu, S.; Low, M.; Zhang, S.-Y.; Liu, Z.; Mlayah, A.; Han, M.-Y. Janus Au-TiO_2 Photocatalysts with Strong Localization of Plasmonic Near-Fields for Efficient Visible-Light Hydrogen Generation. *Adv. Mater.* **2012**, *24*, 2310−2314.
(36) Wu, W.; Liao, L.; Zhang, S.; Zhou, J.; Xiao, X.; Ren, F.; Sun, L.; Dai, Z.; Jiang, C. Non-Centrosymmetric Au-SnO_2 Hybrid Nanostructures with Strong Localization of Plasmonic for Enhanced Photocatalysis Application. *Nanoscale* **2013**, *5*, 5628−5636.
(37) Li, H.; Xia, H.; Wang, D.; Tao, X. Simple Synthesis of Monodisperse, Quasi-spherical, Citrate-Stabilized Silver Nanocrystals in Water. *Langmuir* **2013**, *29*, 5074−5079.

https://dx.doi.org/10.1021/acsomega.0c02818
ACS Omega 2020, 5, 23769−23777

(38) Alexander, G. B.; Heston, W. M.; Iler, R. K. The Solubility of Amorphous Silica in Water. *J. Phys. Chem.* **1954**, *58*, 453−455.
(39) Ivanov, M. R.; Bednar, H. R.; Haes, A. J. Investigations of the Mechanism of Gold Nanoparticle Stability and Surface Functionalization in Capillary Electrophoresis. *ACS Nano* **2009**, *3*, 386−394.
(40) Choi, Y.; Hong, S.; Liu, L.; Kim, S. K.; Park, S. Galvanically Replaced Hollow Au-Ag Nanospheres: Study of Their Surface Plasmon Resonance. *Langmuir* **2012**, *28*, 6670−6676.
(41) Li, E. Q.; Vakarelski, I. U.; Chan, D. Y. C.; Thoroddsen, S. T. Stabilization of Thin Liquid Films by Repulsive van der Waals Force. *Langmuir* **2014**, *30*, 5162−5169.
(42) Kim, T. W.; Lee, D. U.; Choo, D. C.; Yoon, Y. S. Microstructural and Optical Properties of SnO_2 Thin Films Grown on Heavily Doped n-InP(100) Substrates. *Appl. Phys. Lett.* **2001**, *79*, 2187−2189.
(43) Philipse, A. P.; Vrij, A. Preparation and Properties of Nonaqueous Model Dispersions of Chemically Modified, Charged Silica Spheres. *J. Colloid Interface Sci.* **1989**, *128*, 121−136.
(44) Yee, N. Numerical Solution of Initial Boundary Value Problems Involving Maxwell's Equations in Isotropic Media. *IEEE Trans. Antenn. Propag.* **1966**, *14*, 302−307.
(45) Van, P. C.; Surabhi, S.; Quoc, V. D.; Lee, J. W.; Tae, J. W.; Kuchi, R.; Jeong, J.-R. Broadband Tunable Plasmonic Substrate Using Self-assembled Gold-Silver Alloy Nanoparticles. *Curr. Appl. Phys.* **2019**, *19*, 1245−1251.
(46) Uzayisenga, V.; Lin, X.-D.; Li, L.-M.; Anema, J. R.; Yang, Z.-L.; Huang, Y.-F.; Lin, H.-X.; Li, S.-B.; Li, J.-F.; Tian, Z.-Q. Synthesis, Characterization, and 3D-FDTD Simulation of $Ag@SiO_2$ Nanoparticles for Shell-Isolated Nanoparticle-Enhanced Raman Spectroscopy. *Langmuir* **2012**, *28*, 9140−9146.
(47) Oldenburg, S. J.; Averitt, R. D.; Westcott, S. L.; Halas, N. J. Nanoengineering of Optical Resonances. *Chem. Phys. Lett.* **1998**, *288*, 243−247.
(48) Stöber, W.; Fink, A.; Bohn, E. Controlled Growth of Monodisperse Silica Spheres in the Micron Size Range. *J. Colloid Interface Sci.* **1968**, *26*, 62−69.

https://dx.doi.org/10.1021/acsomega.0c02818
ACS Omega 2020, 5, 23769−23777